JACS Au
AN OPEN ACCESS JOURNAL OF THE AMERICAN CHEMICAL SOCIETY

pubs.acs.org/jacsau
Methods/Protocols

The Devil Is in the Details: Pitfalls and Ambiguities in the Analysis of X-ray Powder Diffraction Data of 2D Covalent Organic Frameworks

Samuel Van Gele, Sebastian Bette,* and Bettina V. Lotsch*

Cite This: *JACS Au* 2025, 5, 388−398

Read Online

ACCESS | Metrics & More | Article Recommendations | Supporting Information

ABSTRACT: X-ray powder diffraction (XRPD) data of covalent organic frameworks (COFs) seem to be simple and apparently do not contain a lot of structural information, as these patterns usually do not show more than 3−5 distinguishable Bragg peaks. As COFs are inherently complex materials exhibiting a variety of disorder phenomena like stacking faults, layer curving, or disordered solvent molecules populating the pores, the interpretation of XRPD patterns is far from being trivial. Here we emphasize the critical need for precision and caution in XRPD data acquisition, refinement, and interpretation to avoid common pitfalls and overinterpretations in data analysis. This perspective serves as a comprehensive guide, educating the community on the nuances of refinement processes necessary for advancing COF research with clarity and accuracy.

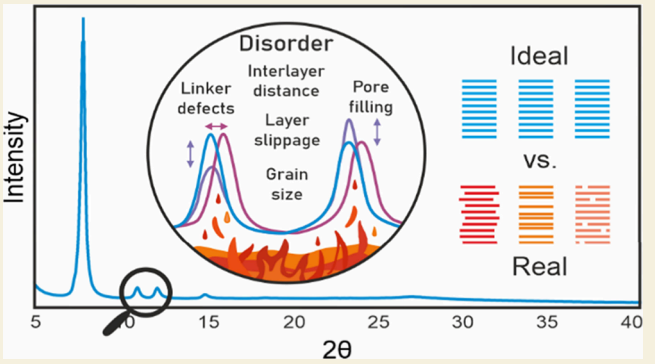

KEYWORDS: *Covalent organic frameworks, XRPD, Refinement, Structure, Defects, Layer stacking*

INTRODUCTION

In recent years, covalent organic frameworks (COFs) have garnered significant attention, owing to their vast potential across various domains, including catalysis, sensing, and gas separation, to name just a few.[1] Through the almost infinite linker library coupled with reticular chemistry strategies, COFs offer a rich tapestry of framework architectures, linkages, and structures.[2−4] COFs are characterized by two main features, notably, their porosity and crystallinity. These are intrinsic structural properties of the material which must be investigated and understood to gain understanding of the COF's structure and properties.

Since their original report in 2005, COFs with a multitude of different linkages, pore geometries and pore sizes have emerged.[5] A typical COF chemist will recognize a COF as a crystalline material through the identification of the (100) and other Bragg peaks in a typical X-ray powder diffraction (XRPD) pattern. With the help of the diffractograms and simulations, a COF chemist will also be familiar with identifying the stacking type of the material, be it an eclipsed (AA) or staggered (AB) arrangement for 2D COFs. In many instances, this might reflect the reality of the structure, however, there are many cases where this "simple" AA or AB image of 2D sheets stacking on top of each other is often reached prematurely without proper investigation of the crystallographic data.

As many 2D materials, COFs are complex and prone to multiple defects such as linkage defects, stacking faults, layer curving, or disordered solvent molecules populating the pores, to name just a few.[6−13] These arise from various factors ranging from linker (non)planarity or flexibility to a multitude of inter- and intralayer interactions (steric, dipole, ionic, hydrogen bonding, and dispersive interactions).

Single crystal COFs have been of interest in recent years with advantages seen in their well-defined structures for in-depth characterization.[14−17] However, most COF materials remain polycrystalline but their characterization data still contain a wealth of unexplored information. The main method for investigating polycrystalline COF structures is through XRPD where the data obtained in diffractograms relate to the frameworks' most often idealized crystalline structure. Common refinement methods such as Pawley or Rietveld help elucidate, build and confirm structural models of COFs. However, it is at this point where information may be lost, over- or misinterpreted and premature structural conclusions are taken, leading to a false image of the material one is working with.

In this perspective, we aim to provide COF chemists with an overview of the refinement methods used in the field and at the same time sensitize for common pitfalls in data interpretation. We will focus on elucidating what aspects of the COFs' structure

Received: October 17, 2024
Revised: November 28, 2024
Accepted: December 2, 2024
Published: December 23, 2024

https://doi.org/10.1021/jacsau.4c00979
JACS Au 2025, 5, 388−398

these methods account for and, just as crucially, their ambiguities. Furthermore, by employing simulations, we will shed light on the intricate factors and structural effects influencing XRPD data in the context of COFs. This way we hope to equip veteran and new researchers in the field with a more profound understanding of the nuances in COF characterization and guide them toward making informed, precise, and scientifically robust conclusions about these intriguing materials.

DEFINITION OF TERMS

A typical diffractogram of a poly crystalline 2D COF consists of 3−5 Bragg peaks mostly at low 2θ angles, each having a specific position, shape and intensity (Figure 1, experimental XRPD

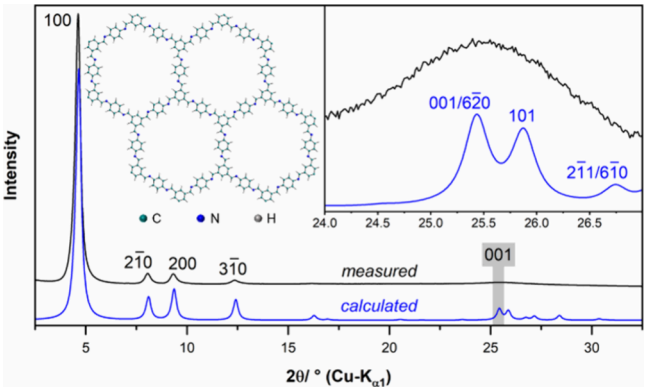

Figure 1. Comparison of the measured (black) and calculated XPRD pattern of COF-LZU1 (molecular model) using a hexagonal structure model with eclipsed layers and empty pores (blue). Selected reflection indices are given. The inset highlights the 001 reflection that corresponds to the interlayer distance.

black line). The low number of diffraction peaks is due to multiple factors such as disorder, porosity, low density, and low structural coherence. The limited number of peaks should, however, not deter researchers from investigating the structure, as substantial information can be extracted despite this apparent limitation.

This paper refrains from delving into an exhaustive exploration of XRPD theory but instead, its primary focus lies in serving as a poignant reminder to readers about the critical significance of refinement methods and the intricate processes and information they encompass. For a deeper exploration into the theoretical intricacies of X-ray diffraction, we guide the reader to the texts by W. Massa,[18] W. Clegg,[19] and R. E. Dinnebier.[20] We wish however to quickly remind the reader of factors giving rise to the information acquired during an XRPD data-collection process.

Peak Positions

The peak positions or 2θ values of diffraction peaks arise from the size, i.e. the lattice parameters, and the metrics of the unit cell. Symmetry elements with a translational component, like lattice centering, glide planes and screw axes, lead to systematic reflection absences. The larger the unit cell, the lower the 2θ values, which is known from the well-known Bragg equation (eq 1). The unit cell contents themselves and their location do not influence the peak positions, but rather their intensities.

Bragg equation:

$$n\lambda = 2d \sin\theta \tag{1}$$

where n is the order of the reflection, λ is the X-ray wavelength, d is the spacing and θ is the incident angle.

Peak Shapes

The peak shapes are determined by the crystallite size, known from the Scherrer equation (eq 2), but also sample microstructure, diffractometer geometry, and instrumental parameters. These parameters can influence if the peak is iso- or aniostropic in nature, for instance.

Scherrer equation:

$$\tau = \frac{K\lambda}{\beta\cos\theta} \tag{2}$$

where τ is the mean size of the ordered domain, K is the shape factor (typically around 0.9), λ is the X-ray wavelength, β is the line broadening at fwhm, and θ is the Bragg angle.

Peak Intensities

The intensities of the diffraction peaks are not arbitrary and are dependent on multiple factors elucidated hereafter:

Scale factor: This factor influences intensities but depends on the experimental parameters used to obtain the diffractograms. Crystallite packing, the amount of diffracting particles, measurement time, instrument parameters - all contribute to the scale factor but remain constant for all peaks in the pattern, thus not affecting the relative peak intensities.

Polarization factor (often combined with the Lorentz factor): The diffraction intensity is dependent on the polarization of the incident X-ray beam which itself is 2θ dependent. In most laboratory set-ups, the X-ray beam is unpolarized. This is different for synchrotron based measurements.

Lorentz factor (often combined with the Polarization factor): The Lorentz factor takes into account multiple effects. It accounts for the θ-dependent changes in the number of X-ray photons that are coherently scattered when the angle slightly diverges off the Bragg condition. It also encompasses the number of crystals that are oriented properly for diffraction to occur, and how much of the diffraction cone intersects with the detector.

Multiplicity factor: The multiplicity depends on the different crystal systems and which, as well as how many, symmetrically equivalent reflections they have. Indeed, if a certain reflection has a high multiplicity, this will increase the peak's intensity.

Absorption: As X-rays travel through a sample measured in transmission or Debye−Scherrer geometry, they are absorbed to a certain extent, which affects peak intensities. The absorption correction is material-, wavelength- and geometry (e.g., the sample thickness)-dependent.

Structure factor: The structure factor, the most influential factor on the peak intensities, tells us about the interference effects that come from atoms located at different positions within the unit cell. This term contains all the information about the atomic positions and their scattering power and greatly influences the intensity of peaks. Identical unit cells containing different atoms or a different arrangement thereof will show Bragg peaks at similar positions but their intensities will be different.

Upon acquisition of experimental data, a COF chemist will build structural models and refine these to the data. Refinement of crystal structures from diffraction data are of key importance

https://doi.org/10.1021/jacsau.4c00979
JACS Au 2025, 5, 388−398

when it comes to determining or evaluating structural models of COFs. Many whole powder pattern fitting methods with and without a structure model are used throughout COF literature, such as Pawley, LeBail and Rietveld refinement, the most common one in the COF field being Pawley refinement. All these methods look at the experimental data and compare its data points to a theoretical diffractogram. The refinements are similar in that they use a "least-squares procedure", a local mathematical optimization method that iteratively adjusts the model to refine the initial structure by minimizing the difference between the observed and calculated diffraction pattern, but widely differ with regards to the parameters contained in each model, as explained in the following.

Single Peak Fit

A single peak fit is sometimes used to refine COF XRPD patterns due the low number of Bragg reflections. This method consists of restricting the refinement to one peak or a set of individual peaks of the diffraction pattern (typically the (100) reflection). From this one peak, it refines the unit cell parameters (a, b, c, α, β, γ), scale factors, background contributions, peak shape parameters and the peak intensity. Such a fitting can be useful in cases where there are only few, low intensity peaks and information about the unit cell size in the layer direction is desirable. It must however be noted that instrument parameters during the refinement can cause the refined peak position to diverge from the actual peak maximum, leading to false unit cell parameters and size.

Pawley Refinement

The Pawley refinement[21] method is the most commonly used refinement method in the COF community. This method, however, does not use a structural model at all. It refines only the metrics of the unit cell, i.e. the unit cell parameters (a, b, c, α, β, γ), scale factors, background contributions, peak shape parameters and peak intensities to fit the peak positions. It is important to note that the Pawley refinement does not refine atomic positions and thus the structure factor and location of the atoms within the unit cell are not considered. The individual peak intensities become refinable, unconstrained parameters, are arbitrary and lose any relation they have to each other. As COF diffractograms have few peaks, it becomes easy to fit them with a simple model, as peaks that could appear in the theoretical model but at a very low intensity can be blown up to match those of the experimental pattern. While a Pawley refinement might be a good start to identify potential unit cell geometries, a perceived "good fit" can easily be obtained and crucial information is lost. Nevertheless, the parameter correlation matrix can contain valuable information.

A further step one may take is performing a Pawley refinement with an internal standard with known lattice parameters (e.g., such as corundum or diamond powder) which offers reflections at large 2θ. Having an internal standard allows for the suppression of zero shift error which can lead to artificial distortion of the COF lattice parameters.

Le Bail Refinement

Le Bail refinement[22] is similar to Pawley refinement with regard to the parameters utilized, but differs in the algorithm used to reach convergence, e.g. positive peak intensities are enforced by the algorithm. Most importantly, it yields the same information as a Pawley refinement (i.e., lattice parameters) and suffers from the same drawbacks.

Rietveld Refinement

The Rietveld refinement[23−25] method is rarely used in the COF community, while it is the most powerful of all refinement methods by far. It is a full structural model comprising atomic positions, thermal displacement parameters, and occupancy factors to describe the crystal structure. The Rietveld method actively refines the unit cell metrics (a, b, c, α, β, γ), scale factors, background contributions, peak shape parameters and the atomic positions of those contained within the unit cell. The intensities are not a refinable parameter. They are calculated based on the contents of the unit cell (structure factor) and thus peak intensity relations within a diffractogram are maintained, which is crucial structural information.

The quality of the XRPD data refinement is indicated by several figures of merit:

Weighted Profile Reliability Factor (R_{wp})

This factor assesses the agreement between the observed and calculated diffraction patterns. It takes into account not just the individual intensity or amplitude of the diffraction peaks but also considers the uncertainties or errors associated with these intensities. The R_{wp} incorporates a weighting scheme, which assigns different weights to data points based on their reliability or measurement error. It should be noted that the R_{wp} also takes the fit of the background into account. Hence fitting XRPD data with a background consisting of many background polynomials leads to a low R_{wp} value even if a poor or unsuitable model is used. All conventional refinement programs calculate background corrected R_{wp} values, e.g. usually denoted as "R_{wp}_dash". As these are considerably higher than the plain R_{wp} values, they are usually not reported in the literature.

Expected Reliability Factor (R_{exp})

This factor is calculated based on the degrees of freedom in the refinement process, considering the number of reflections, the experimental errors and the errors in the detector's counting statistics. It provides a baseline or target value for the R-factor that one might expect to achieve if the model perfectly represents the crystal structure given the experimental data quality. If the errors in the detector's counting statistic are not included into the raw data by default, most refinement software tries to estimate them by the noise in the data, which usually leads to a tremendous underestimation of the R_{exp} value and therefore to an artificially large GOF (see below).

Goodness of Fit (GOF or GooF)

Refinements are usually characterized by their goodness of fit. In powder X-ray diffraction refinement methods, the GOF is determined by the ratio between the weighted profile reliability factor, R_{wp}, and the expected reliability factor, R_{exp}. A GOF of 1.0 is considered as ideal. For XRPD data GOF values between 2 and 3 are regarded as acceptable. A large GOF may indicate a poor fit or might be attributed to an overestimation of the counting statistics (see above). A GOF value of smaller than 1 indicates an overparametrization of the refinement. It is important to note that the GOF does not give any indication of whether a structural model is crystallographically and chemically reasonable or not.

STRUCTURAL EFFECTS INFLUENCING COF XRPD PATTERNS

Having recalled the data analysis approaches of XRPD patterns of COF materials, we would now like to exemplify how various structural effects are reflected in obtained diffraction patterns. It

https://doi.org/10.1021/jacsau.4c00979
JACS Au 2025, 5, 388−398

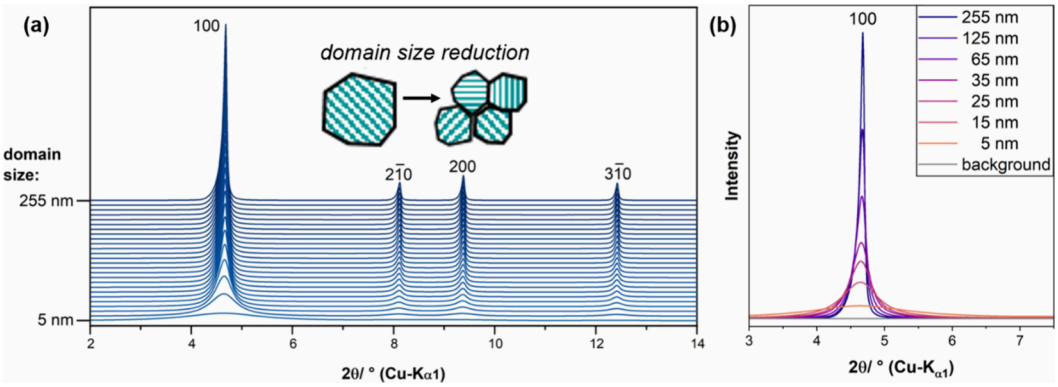

Figure 2. (a) Series of simulated XRPD patterns of COF-LZU1 with an iterative reduction of the domain site from 255 to 5 nm in 10 nm steps. Including selected reflection indices. (b) Close-up of the 100 reflection with different degrees of domain size-related peak broadening.

must be noted that XRPD patterns of COF materials are inherently difficult to analyze as they only show very few reflections and seem to contain little information, however a deeper understanding of COF structures is realistically attainable nevertheless.

Here, we will focus on a chemically simple COF system, COF-LZU1 (1,3,5-triformylbenzene - p-phenylenediamin COF) (Figure 1, experimental XRPD black line) and investigate various structural effects that may influence the experimental pattern.

Furthermore, an additional example, COF-366-Co, is presented in the Supporting Information (Supporting Information S1). We show step-by-step how Pawley refinements can lead to erroneous structural assignments. COF-366-Co is known for its electrocatalytic properties, and correct structural elucidation is key as a first step to understanding structure–property relationships.

The pattern of COF-LZU1 is dominated by the very intense 100 reflection, which is attributed to the lateral (i.e., in-plane) dimension of the unit cell. Three additional, weak reflections are visible: 2$\bar{1}$0, 200 and 3$\bar{1}$0, similarly associated with the lateral dimension of the unit cell. Reflections attributed to the interlayer distance (like 001) seem to be absent (Figure 1, gray background). Upon closer inspection, however, it can be seen that they are not entirely absent. Instead, a broad hump is situated at the expected reflection position (Figure 1, inset). Note that this hump cannot be assigned to the 001 reflection unambiguously, as the 6$\bar{2}$0 and 101 reflections are located in close proximity. Hence it is obvious that the lateral dimension of the COF unit cell can be derived directly from the XRPD pattern, whereas the precise interlayer distance cannot be determined, which is a common phenomenon in other COF systems as well. In consequence, the performance of meaningful crystal structure refinements of COFs using XRPD patterns to extract 3D structural information is difficult.

The difficulty in the analysis becomes clear when we compare the experimentally measured XRPD pattern of COF-LZU1 with a calculated pattern assuming eclipsed stacking and empty pores (Figure 1, blue line). The position of the 100, 2$\bar{1}$0, 200 and 3$\bar{1}$0 reflections exhibit a very good match between both measured and calculated patterns. The ratio of the peak maxima between the 100 peak and the 2$\bar{1}$0, 200 and 3$\bar{1}$0 reflections, however, is significantly smaller in the measured pattern. Moreover, the calculated pattern shows sharp Bragg peaks at diffraction angles $2\theta > 15°$ (Figure 1), whereas the measured pattern does not. The mismatch between measured and calculated diffraction patterns primarily originates from the "real" structure—as opposed to the ideal or average structure—of the COF that gives rise to many different types of structural defects.

In the following we will demonstrate how different crystal structure defects which can occur in COF materials, such as grain size, pore filling, stacking order, interlayer arrangements and linker defects, affect XRPD patterns using COF-LZU1 as an example.

All simulations were performed using Cu–$K_{\alpha 1}$ radiation, which is typically used for X-ray powder diffraction of COF-materials, and the instrumental profile of a STOE-Stadi-P diffractometer in Debye–Scherrer geometry. It should be noted that structural defects can materialize in different degrees. Therefore, rather than the exact match between simulated and measured patterns, we will focus on the interpretation of trends in changes of the peak shapes and intensities. Details on the setup of the XRPD data simulations can be found in the Supporting Information.

DOMAIN SIZE

In the literature, COFs are often denoted as "crystalline" when rather sharp and intense Bragg peaks are visible and "semi-crystalline" or "non-crystalline", when they are broad or (nearly) absent. The term "crystallinity" refers to the presence of coherently scattering domains, i.e. crystallites in which a regular, 3-dimensional periodic arrangement of atoms exists. Thus, crystallite size (or the size of coherently scattering domains) has a stark influence on the XRPD pattern. In Figure 2, we present a series of simulated XRPD patterns of COF-LZU1 in which we gradually reduce the mean size of the coherently scattering domains from 255 to 5 nm (corresponding to 155 × 155 and 2 × 2 repeating units, respectively). For large domain sizes, the peaks exhibit an anisotropic shape, i.e. tailing toward lower diffraction angles, which is typical for XRPD data collected in Debye–Scherrer geometry. Accordingly, the peak shape is governed by the instrumental profile. A significant reduction of the domain size from 255 to 65 nm, leads to some peak broadening, which is associated with a significant reduction of the peak maximum (Figure 2b). The reflections still exhibit an anisotropic shape. Further reduction of the mean domain size leads to additional peak broadening and a transition to a more Gaussian-like, i.e. symmetrical, shape. In consequence, for small average domain sizes, the peak profile is governed by the mean domain size. At an average domain size of 5 nm the peak broadening is extremely pronounced and the reflection almost merges with the background. It must be noted that a small average domain

https://doi.org/10.1021/jacsau.4c00979
JACS Au 2025, 5, 388–398

size, which can be described as being diagnostic of low crystallinity, leads to peak broadening and a decrease in the peak maximum. The reflection intensity, i.e. the integral area underneath a diffraction line, is not affected. If the background (Figure 2b, gray line) of an XPRD pattern is known, these peaks might be still identified.

LAYER SLIPPAGE

Another aspect of the COF crystal structures, which is often controversially discussed in the literature, is the layer arrangement, i.e. the stacking order of the COF layers.[11,26−29] The initial simulation (Figure 3, blue line) was performed using a fully eclipsed stacking of the layers (AA stacking), although there is ample evidence that a perfectly eclipsed stacking does not exist in COFs.[6,9,30] Instead, a stacking order in which subsequent layers have some small offset within the *ab*-plane with regard to the preceding layer (few Angstroms), quasi AA-stacking, is assumed to be present in most COFs due to an overall lowering in the energetics of such a configuration.[27,28] Stacking has also been shown to have numerous influences on COF properties.[31−37]

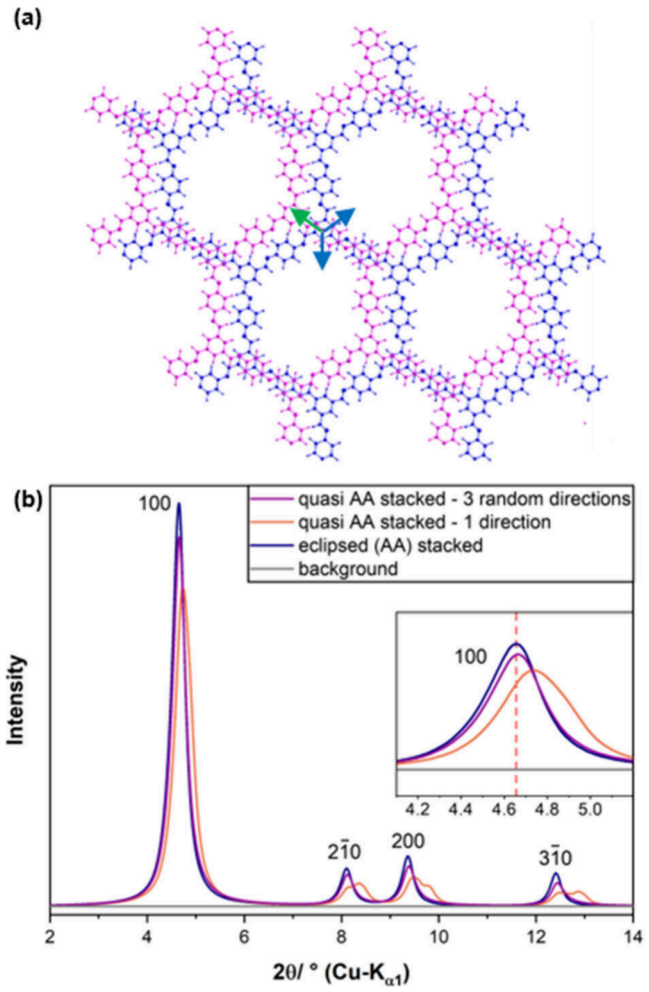

Figure 3. (a) Structure model of a bilayer of COF-LZU1 showing the bottom layer in blue and the top layer in magenta. The projection of the stacking vector onto the *ab*-plane is represented by the green arrow. Slippage can happen simultaneously along any direction indicated by green and blue arrows. (b) Simulated XRPD patterns using different stacking orders.

Layer slippage can happen in different ways and different stacking polymorphism and planar disorder have significant effects on XRPD patterns.[38] In our example, if the subsequent COF layers are unidirectionally slipped by 1 Å (Figure 3a, green arrow), then the 100 reflection is shifted toward higher diffraction angles and the 2$\bar{1}$0, 200 and 3$\bar{1}$0 become split (Figure 3b, blue and orange lines) due to a loss of the hexagonal lattice symmetry.[39] This effect is clearly detectable in the diffraction patterns.

The node of COF-LZU1, however, exhibits a trigonal molecular symmetry leading to a trigonal layer symmetry, which is also apparent in many other hexagonal COFs. As a consequence, the layer slipping can occur in any of the three directions that are equivalent by layer symmetry (Figure 3a, green and blue arrows). Hence, the layer slipping is most likely to occur randomly among these three directions. The simulated diffraction pattern of a multidirectional random layer slipping (Figure 3b, violet line) is almost identical to the diffraction pattern of a fully eclipsed stacked COF (blue line). A slight anisotropic peak broadening leads to a small shift of the peak maxima that might be easily overlooked and compensated by using an artificially smaller *a*- and *b*-unit cell axis or refining the zero error of the diffractometer.

In COF-LZU1, the offset of the layer slipping within the *ab* plane is not predetermined by any feature of the structure of the COF-layer. Accordingly, we performed a series of simulations in which we incrementally increased the layer offset using a 3-directional, randomized slipped stacking order from 0 to 5 Å (Figure 4). For comparatively small layer offset of ≤2 Å, the XRPD patterns exhibit close similarity with the simulated pattern of an eclipsed stacked structure (Figure 4b). The anisotropic peak broadening causes a slight shift of the peak maxima. If the layer offset is further increased, the anisotropic diffraction line broadening becomes more pronounced and the 2$\bar{1}$0, 200 and 3$\bar{1}$0 reflections finally merge with the background (Figure 4a) and the 100 reflection adopt a very characteristic triangular peak shape, a so-called Warren-type peak.[40] It should be noted that the larger the lateral dimension of the COF, the more the peak broadening effect of the layer offset is reduced, i.e. large COFs can show larger layer offsets while exhibiting less pronounced anisotropic peak broadening such as large pore polyimide COF PI-COF-3[41] or PP-TAPB COF.[30] In consequence, the detection of a randomized slipped stacking becomes more difficult the larger the COF. Moreover, as the offset distance is not templated by the chemical structure of the COF itself, it also could be randomized, which would lead to a peak broadening due to a reduction of the structural coherence on its own. Accordingly, determining a mean layer offset from XRPD data is far from being trivial and often only rough approximations or semiquantitative trend analyses are possible but further methods such as PDF analysis might offer deeper insights.[30]

PORE FILLING

Another aspect of COF structures that can make crystal structure analyses more complicated are the pores; specifically, their content. COFs exhibit pore volumes of more than 50% of the total volumes and these structures are not stable at ambient conditions if the pores are vacant.[42] Under ambient conditions, the COF pores are filled with disordered solvent, water molecules, or gas.[13] Despite the delocalized character of the electron density of the guest molecules within the pores, they can have a significant impact on the XRPD pattern.[28] It should

https://doi.org/10.1021/jacsau.4c00979
JACS Au 2025, 5, 388−398

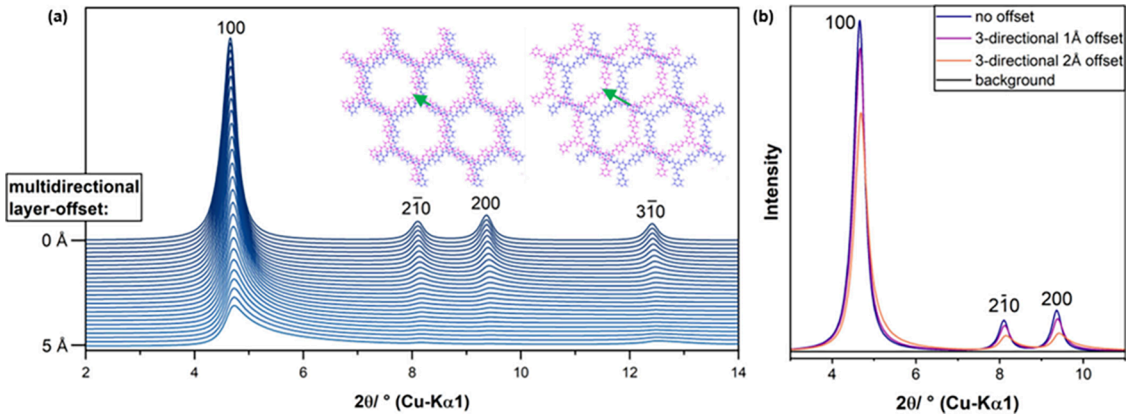

Figure 4. (a) Series of simulated XRPD patterns of COF-LZU1 showing a random 3-directional slipped stacking order in which the layer offset was incrementally increased from 0 to 5 Å. (b) Close-up of the low 2θ range of the XRPD pattern showing the simulated pattern for no layer offset and for layered offsets of 1 and 2 Å.

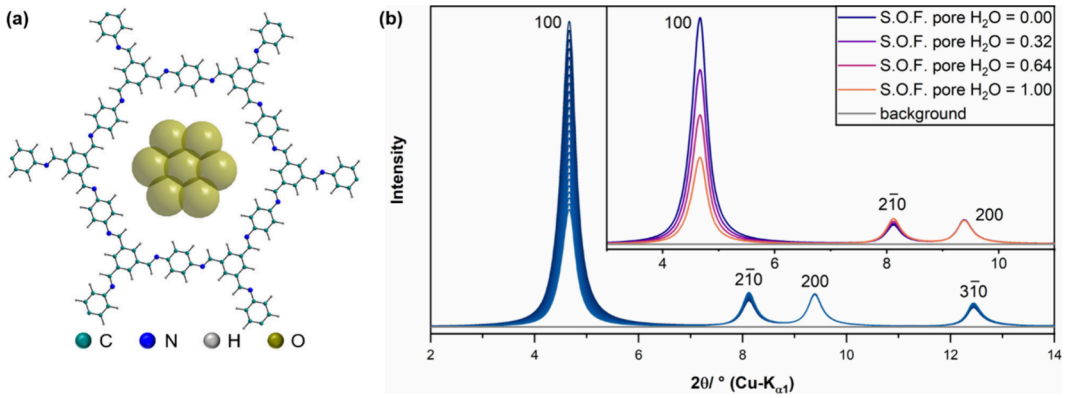

Figure 5. (a) Illustration of COF-LZU1 structure model that was used for the simulations: randomized 3-directional layer offset by 1 Å, pores filled with 7 oxygen atoms mimicking water or solvent using 3-fold increased thermal displacement parameters for simulating positional disorder. (b) Series of simulated XRPD patters with an iterative increase in the site occupancy factor (SOF) of the host atoms within the pores, in the inset, the low 2θ angle region is shown for selected pattern for clarity.

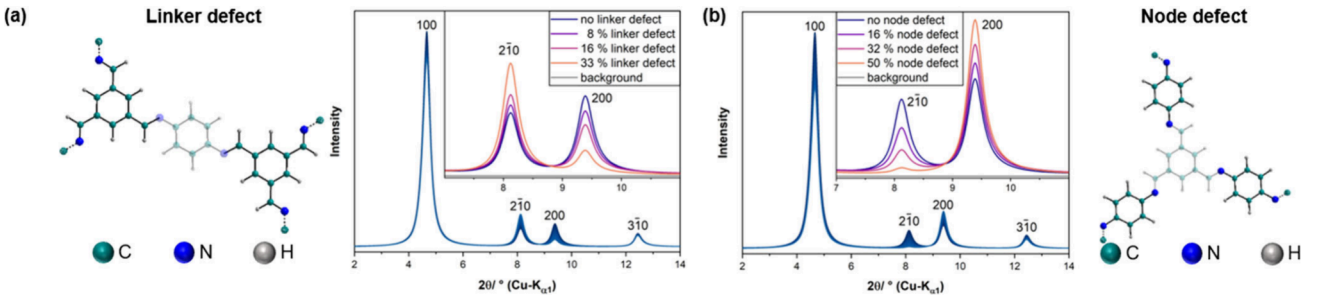

Figure 6. Simulated XRPD patterns of COF-LZU1 structure implementing an increasing amount of (a) linker and (b) node defects.

be noted that if a COF is stored under argon atmosphere and if it takes up argon gas, the absorbed gas molecules have a significant impact on the XPRD pattern due to the stronger scattering power of argon. For comprehensive simulations we used COF-LZU1 with a 3-directional randomized slipped structure applying a mean layer offset of 1 Å. Seven oxygen atoms mimicking water or solvent molecules were placed within the pores applying a 3-fold increased thermal displacement parameter representing positional disorder of the guest molecules (Figure 5a). During the series of simulations (Figure 5b), we iteratively increased the site occupancy factors (SOF) of the guest atoms. An increase of the degree of pore filling leads to a significant decrease of the peak intensity of the 100 reflection and to lesser extent of 2$\bar{1}$0 and 3$\bar{1}$0 peaks due to a decrease in scattering contrast. Since the disordered solvent molecules often have similar scattering power as the pore walls, solvent incorporation leads to an increase in cell symmetry by the creation of a pseudo subcell, which is associated with a decrease of the diffraction line intensity.[13] For larger COFs this effect can be even more pronounced and can lead to an extinction of the 100 reflection.[13] If the incorporated guest molecules are not ordered, they do not break the symmetry of the crystal structure. In consequence, no new diffraction lines appear and solvent incorporation does not lead to peak broadening. Due to a pronounced correlation between site occupancy and positional disorder (often modeled by large thermal displacement

https://doi.org/10.1021/jacsau.4c00979
JACS Au 2025, 5, 388−398

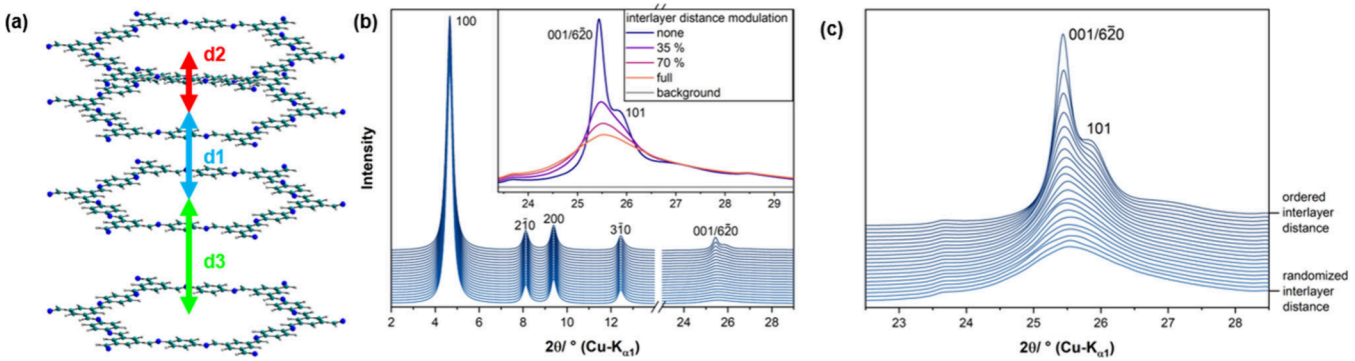

Figure 7. (a) Illustration of the appearance of different interlayer distances (d1, d2, d3) in the structure of COF-LZU1 exhibiting stacking in a 3-directonal randomized slipped stacking order. (b) Series of simulated XRPD patterns with an iterative randomization of the interlayer distance using three distinct interlayer distances: d1 = 3.5 Å, d2 = 3.0 Å, and d3 = 4.0 Å with selected XRPD patterns are presented in the inset (enlarged by a factor of 20). (c) High 2θ angle region of the series of simulated XRPD patterns (enlarged by a factor of 20) with an iterative randomization of the interlayer distance.

parameters) of the host molecules, the absolute occupancy of the pores cannot be extracted directly from the diffraction patterns. Accordingly, XRPD data interpretation has to be limited to the description of semiquantitative trends, e.g. by comparing similar samples or analyzing *in situ* data, and should be correlated with complementary analyses such as sorption measurements.[13]

LINKER AND NODE DEFECTS

Another type of possible disorder in the constitution of the COF layers are linker and node defects (Figure 6), caused, e.g., by incomplete polymerization reactions. If these defects are distributed absolutely randomly across the crystal structure, they do not break the crystal symmetry, hence they do not lead to diffraction line broadening or the appearance of new Bragg peaks. Instead, these point defects cause a reduction of certain peak intensities. In the COF-LZU1 structure linker (p-phenylenediamine) defects cause a small reduction of the 100 peak intensity and a significant reduction of the 200 diffraction line intensity, whereas the intensity of the 2$\bar{1}$0 peak increases (Figure 6, a). Node (1,3,5-triformylbenzene) defects, in contrast, lead to almost opposite effects: the 100 peak intensity slightly decreases as well, but the 200 diffraction line intensity increases, whereas the 2$\bar{1}$0 peak intensity decreases. Thus, in theory, node defects can be distinguished from linker defects in the COF-LZU1 structure; however, it appears likely that both node and linker defects occur simultaneously. Depending on the type of COF investigated and on the degree of pore filling, these two types of point defects can either cancel each other's effect on the XRPD pattern or may lead to a decrease in 200 and 2$\bar{1}$0 peak intensity relative to the 100 diffraction line intensity.

INTERLAYER DISTANCE

Up to this point, our considerations have covered the low 2θ angle region of the XRPD patterns and the reflections that are usually visible in the diffraction patterns of crystalline COFs. But as we initially showed, there is no sharp 001 reflection attributed to the interlayer distance in the measured COF XRPD patterns, instead, only a broad hump is visible (Figure 1, inset). This indicates a loss of structural coherence perpendicular to the layer plane, i.e. a random modulation of the interlayer distance throughout the structure. There are a variety of possible origins for such a modulation, such as pore filling caused by guest-COF interactions, disorder within linker molecules if they exhibit rotational degrees of freedom, or layer buckling.[30] For a series of XRPD pattern simulations we chose two additional interlayer distances: d2 = 3.0 Å and d3 = 4.0 Å along with the expected interlayer distance of d1 = 3.5 Å (Figure 7a). Then, we iteratively randomized the interlayer distance in a symmetrical way (i.e., a shift toward d2 is as likely as a shift toward d3) and implemented this into the COF-LZU1 structure with a 3-directional randomized slipped stacking order. The 2θ angle region below 15° is not affected by the random modulation of the interlayer distance as there are only *h*00 and *hk*0 reflections (Figure 7b). At higher 2θ angles, the modulation of the interlayer distance has a significant impact on the diffraction patterns (Figure 7c). The interlayer distance was modulated both toward smaller and larger distances to the same extent, i.e. the mean interlayer distance is not changed nor is the position of the 001. Instead, this peak, as well as the 101 reflection, is symmetrically broadened. As the 6$\bar{2}$0 reflection exhibits broadening from the randomization of the direction of the slipped stacking, all three largely broadened peaks merge to one hump that strongly resembles the measured XRPD pattern within the same 2θ range (Figure 1, inset). It must be noted that an unsymmetrical modulation of the interlayer distance either toward smaller or larger distances will change the mean interlayer distance and therefore shift the maximum of the broadened peak accordingly. In addition, an asymmetric peak broadening, which can materialize in a triangular peak shape, also occurs.[30] In consequence, refining the position of the 001 peak-related hump will only give information on the mean interlayer distance, which is usually associated with a large uncertainty due to the overall broad and complicated peak shape.

ADDITIONAL DEFECTS

Another important fault type is layer buckling, which is not trivial to simulate properly in direct space since it requires to iteratively change the unit cell metrics with degree of buckling while maintaining the intralayer connectivity and therefore will not be shown in detail. Nevertheless, it has been investigated extensively in the literature and was shown to lead to a shrinking of the ab-plane of the unit cell, which was accompanied by significant peak broadening.[30,43,44]

In summary, we simulated the effects of the most obvious types of disorder in COF materials on the XRPD patterns. The different types of disorder lead to changes in the peak shape, mean peak positions, peak maxima and integral peak intensities.

https://doi.org/10.1021/jacsau.4c00979
JACS Au 2025, 5, 388−398

Due to the flexible and often poorly defined nature of the COF structures, several types of structural disorder can be expected to occur simultaneously, leading to a combined impact on the XRPD pattern. Hence extracting precise structural information, even very basic ones, such as the lateral dimension of the unit cell, is not trivial and deconvolution of the individual disorder parameters has to be done with great care.

Even though sometimes ambiguous, we would like to note that XRPD is a potentially powerful tool to help in guiding synthesis toward more atomically precise crystalline materials. Within identical COF systems, the analysis of PXRD parameters such as peak fwhm, counts and precise peak positions (obtained with internal standards) can offer avenues to exploring COF microstructures through the optimization of synthetic conditions or introduction of specific chemical groups as we have previously shown.[30]

RECOMMENDATIONS AND COMPLEMENTARY METHODS

Against the backdrop of decades of polymer chemistry, the synthesis of crystalline 2D COF materials has materialized only relatively recently. Gaining a comprehensive understanding of their average and real structures is the next big frontier in this endeavor.

As we have demonstrated above, many factors and real structure effects have a profound influence on their powder diffraction patterns, rendering the characterization of COFs a challenging task. To enhance the quality and reliability of data obtained through X-ray powder diffraction (XRPD), we propose the following guidelines:

(1) Crystallinity is not trivial to define for COFs and the lines between them and porous polymers can in some cases be blurred. Contrary, to traditional polymer chemistry, which benefits from concrete measurable parameters to describe the system such as M_n, M_w and the PI, the precise nanostructures in COFs (mean sheet size, mean sheet stacking, shape factors, edge functionalities) remains elusive.[45] However, in instances where the material under investigation does not exhibit crystallinity (i.e., the presence of at least a sharp diffraction peak), it advisible to refrain from categorizing such materials as COF.

(2) When presenting XRPD diffractograms, it is advisible to include not only the experimental and refined data, but also the diffraction pattern corresponding to the unrefined structural model.

(3) Researchers should possess a thorough understanding of the specific information contained within each refinement method. A Pawley refinement, is considered less robust compared to a Rietveld refinement as it only provides unit cell metrics and not any atomic level structural information. The inability to achieve an ideal fit using Rietveld refinement does not inherently undermine the validity of the structure. However, drawing conclusions regarding structure−property relationships in the absence of a well-defined model is not advisible.

(4) COFs often exhibit various real structure effects and disorder scenarios that can significantly affect diffraction data as seen above. Researchers should be aware of these disorder phenomena, as they play a crucial role in the refinement process, impacting the quality and reliability of the obtained results.

(5) Understanding the scattering contributions from pore filling is imperative. The presence or not of guest molecules within the pores can drastically change the ratios between peak intensities in the diffractogram as it may only affect certain peaks. This change can lead to inconclusive refinements as the structure factor calculated during Rietveld differs largely between solvent-free and pore-filled COFs. Recognizing this helps in distinguishing between the structural information on the framework and the guest molecules, contributing to a more accurate analysis of COFs.

In addition to these recommendations, we also suggest investigating other analytical techniques that may offer insight into the material's structure:

***In situ* XRPD** methods offer a dynamic perspective, allowing for real-time observation of changes in materials under varying conditions. These methods encompass a range of experimental setups, such as temperature-controlled environments, pressure cells, gas flow, or humidity chambers. By coupling XRPD with these techniques, one can gain insights into structural modifications, phase transitions, or reactions occurring within a material as it undergoes external stimuli. For instance, monitoring crystalline phase transitions during heating or observing structural changes under humidity changes can provide invaluable information about a material's behavior and stability.[13,30,46] This integrative approach not only validates XRPD data but also broadens the scope of understanding materials' properties and functionalities, enhancing the overall reliability and applicability of the obtained results.

Sorption measurements, already a central tool in the characterization of COFs, can be used to gain insight into pore size and volume. We previously showed how such a method may be complementary in confirming layer slipping in 2D COFs.[30] This method, coupled with simulations, helps to build a more defined picture of the structure and its porosity, which are crucial to applications such as catalysis, gas storage, and separation.[6]

Solid-state NMR, for example, can provide valuable insights into local atomic environments and chemical bonding, providing details on local structure effects that XRPD cannot.

Total scattering and PDF-analysis can also offer valuable insights into the local structure and stacking disorder in COF materials beyond the average view of XRPD.[9,47] This method is far from trivial as quality data acquisition usually requires a synchrotron source and data reduction and analysis bring their own challenge, but can yield great insights into the structure.

CONCLUSION

COF materials are an extremely interesting and versatile class of reticular materials offering a broad range of applications as well as a platform to understand and explore 2D materials and confinement effects in porous materials. Herein, we recall the different parameters utilized in various structural refinement methods and show that the structural elucidation of 2D COFs is far from trivial. Many factors such as grain size, layer slippage, guest molecules, linker defects and a spread in interlayer distances can have a large influence on the obtained diffractogram of a COF material. Being aware of these effects is key to perform high quality structural refinements to gain an idea of the real COF structure beyond the typical AA or AB image. Simulations performed on a structural model of COF-LZU1 showed that peak positions, intensities and symmetry are all

https://doi.org/10.1021/jacsau.4c00979
JACS Au 2025, 5, 388−398

affected by these numerous effects and even subtle deviations between simulated diffractograms and experimental data could hint at disorder, which is naturally present in these materials. Understanding the influence of defects on PXRD patterns is vital for accurate structural elucidation. However, researchers should not allow these challenges to overshadow efforts to optimize synthetic conditions for obtaining high-quality crystalline samples. We invite the readers to explore a further example of structural ambiguity with COF-366-Co in the Supporting Information to this text.

METHODS

Structure modeling and Rietveld refinement were performed with BIOVA Materials Studio 2017 (17.1.0.48. Copyright 2016 Dassault Systèmes) software and its Reflex module.

Simulations of COF-LZU1

The program TOPAS v6.0[48] was used for all simulation of XRPD patterns as described elsewere.[49] For the simulations, we used the instrumental profile of a Stoe Stadi P powder diffractometer in Debye−Scherrer geometry (Cu−Kα1 radiation from primary Ge(111)-Johann-type monochromator, triple array of Mythen 1 K detectors (Dectris)) modeled by using the fundamental parameter approach[50,51] as implemented into the TOPAS software. Parameters like domain size, fault probability or length of the stacking vector were iteratively varied throughout a series of simulations using previously published grid search routines.[52,53]

Refinements of COF-366-Co

Pawley and Rietveld refinements were performed using TOPAS v6.0.[48] The background was modeled with Chebychev polynomials with the order indicated in the respective refinements. Simple axial and zero-error corrections were used together with additional corrections for Lorentzian crystallite size and/or strain broadening.

General Methods

All reactions were performed without magnetic stirring. Unless otherwise noted, reagents were purchased from different commercial sources and used without further purification.

Infrared Spectroscopy

IR spectra were recorded on a PerkinElmer UATR Two FT-IR spectrometer equipped with an attenuated total reflection (ATR) measuring unit. IR data are reported in wavenumbers (cm^{-1}) of normalized absorption.

XRPD

X-ray powder diffraction experiments were performed on a Stoe Stadi P diffractometer (Cu−Kα1, Ge(111) in Debye−Scherrer geometry. The samples were measured in sealed glass capillaries (OD = 1.0 mm) and spun for improved particle statistics.

ASSOCIATED CONTENT

Data Availability Statement

The data that support the findings of this study are available in the Supporting Information of this article. The primary data before processing are available in the repository DaRUS (10.18419/darus-4588).

Supporting Information

The Supporting Information is available free of charge at https://pubs.acs.org/doi/10.1021/jacsau.4c00979.

Additional example of structural elucidation with COF-366-Co, detailed synthetic procedures, FT-IR spectra, XRPD patterns (PDF)

AUTHOR INFORMATION

Corresponding Authors

Bettina V. Lotsch − *Max Planck Institute for Solid State Research, 70569 Stuttgart, Germany; Department of Chemistry, Ludwig-Maximilians-Universität (LMU), 81377 Munich, Germany;* orcid.org/0000-0002-3094-303X; Email: b.lotsch@fkf.mpg.de

Sebastian Bette − *Max Planck Institute for Solid State Research, 70569 Stuttgart, Germany;* orcid.org/0000-0003-3575-0517; Email: s.bette@fkf.mpg.de

Author

Samuel Van Gele − *Max Planck Institute for Solid State Research, 70569 Stuttgart, Germany; Department of Chemistry, Ludwig-Maximilians-Universität (LMU), 81377 Munich, Germany*

Complete contact information is available at: https://pubs.acs.org/10.1021/jacsau.4c00979

Author Contributions

The manuscript was written through contributions of all authors. All authors have given approval to the final version of the manuscript.

Funding

Financial support by an ERC Starting Grant (project COF Leaf, Grant No. 639233), the Deutsche Forschungsgemeinschaft (DFG, Project-ID 358283783 - SFB 1333), the Max Planck Society, the Cluster of Excellence e-conversion (Grant No. EXC2089), and the Center for Nanoscience (CeNS) is gratefully acknowledged.

Notes

The authors declare no competing financial interest.

ACKNOWLEDGMENTS

The authors would like to thank Lars Grunenberg, Fabian Heck and Amelie Heilmaier for their discussions and for reading the manuscript, as well as Robert E. Dinnebier for his insightful comments on the manuscript.

ABBREVIATIONS

COF, covalent organic framework; GOF, goodness of fit; R_{exp}, expected reliability factor; R_{wp}, weighted profile reliability factor; XRPD, X-ray powder diffraction; Mw, weight-average molecular weight; Mn, number-average molecular weight; PI, polydispersity Index

REFERENCES

(1) Freund, R.; Zaremba, O.; Arnauts, G.; Ameloot, R.; Skorupskii, G.; Dincă, M.; Bavykina, A.; Gascon, J.; Ejsmont, A.; Goscianska, J.; Kalmutzki, M.; Lächelt, U.; Ploetz, E.; Diercks, C. S.; Wuttke, S. The Current Status of MOF and COF Applications. *Angew. Chem., Int. Ed.* **2021**, *60* (45), 23975−24001.

(2) Lohse, M. S.; Bein, T. Covalent Organic Frameworks: Structures, Synthesis, and Applications. *Adv. Funct. Mater.* **2018**, *28* (33), 1705553.

(3) Geng, K.; He, T.; Liu, R.; Dalapati, S.; Tan, K. T.; Li, Z.; Tao, S.; Gong, Y.; Jiang, Q.; Jiang, D. Covalent Organic Frameworks: Design, Synthesis, and Functions. *Chem. Rev.* **2020**, *120* (16), 8814−8933.

(4) Tan, K. T.; Ghosh, S.; Wang, Z.; Wen, F.; Rodríguez-San-Miguel, D.; Feng, J.; Huang, N.; Wang, W.; Zamora, F.; Feng, X.; Thomas, A.; Jiang, D. Covalent Organic Frameworks. *Nat. Rev. Methods Primer* **2023**, *3* (1), 1−19.
(5) Côté, A. P.; Benin, A. I.; Ockwig, N. W.; O'Keeffe, M.; Matzger, A. J.; Yaghi, O. M. Porous, Crystalline, Covalent Organic Frameworks. *Science* **2005**, *310* (5751), 1166−1170.
(6) Kessler, C.; Schuldt, R.; Emmerling, S.; Lotsch, B. V.; Kästner, J.; Gross, J.; Hansen, N. Influence of Layer Slipping on Adsorption of Light Gases in Covalent Organic Frameworks: A Combined Experimental and Computational Study. *Microporous Mesoporous Mater.* **2022**, *336*, 111796.
(7) Cairns, A. B.; Goodwin, A. L. Structural Disorder in Molecular Framework Materials. *Chem. Soc. Rev.* **2013**, *42* (12), 4881.
(8) Sick, T.; Rotter, J. M.; Reuter, S.; Kandambeth, S.; Bach, N. N.; Döblinger, M.; Merz, J.; Clark, T.; Marder, T. B.; Bein, T.; Medina, D. D. Switching on and off Interlayer Correlations and Porosity in 2D Covalent Organic Frameworks. *J. Am. Chem. Soc.* **2019**, *141* (32), 12570−12581.
(9) Pütz, A. M.; Terban, M. W.; Bette, S.; Haase, F.; Dinnebier, R. E.; Lotsch, B. V. Total Scattering Reveals the Hidden Stacking Disorder in a 2D Covalent Organic Framework. *Chem. Sci.* **2020**, *11* (47), 12647−12654.
(10) Martínez-Abadía, M.; Mateo-Alonso, A. Structural Approaches to Control Interlayer Interactions in 2D Covalent Organic Frameworks. *Adv. Mater.* **2020**, *32* (40), 2002366.
(11) Huang, J.; Shin, S.-J.; Tolborg, K.; Ganose, A. M.; Krenzer, G.; Walsh, A. Room-Temperature Stacking Disorder in Layered Covalent-Organic Frameworks from Machine-Learning Force Fields. *Mater. Horiz.* **2023**, *10* (8), 2883−2891.
(12) Kang, C.; Zhang, Z.; Wee, V.; Usadi, A. K.; Calabro, D. C.; Baugh, L. S.; Wang, S.; Wang, Y.; Zhao, D. Interlayer Shifting in Two-Dimensional Covalent Organic Frameworks. *J. Am. Chem. Soc.* **2020**, *142* (30), 12995−13002.
(13) Grunenberg, L.; Savasci, G.; Emmerling, S. T.; Heck, F.; Bette, S.; Cima Bergesch, A.; Ochsenfeld, C.; Lotsch, B. V. Postsynthetic Transformation of Imine- into Nitrone-Linked Covalent Organic Frameworks for Atmospheric Water Harvesting at Decreased Humidity. *J. Am. Chem. Soc.* **2023**, *145* (24), 13241−13248.
(14) Evans, A. M.; Parent, L. R.; Flanders, N. C.; Bisbey, R. P.; Vitaku, E.; Kirschner, M. S.; Schaller, R. D.; Chen, L. X.; Gianneschi, N. C.; Dichtel, W. R. Seeded Growth of Single-Crystal Two-Dimensional Covalent Organic Frameworks. *Science* **2018**, *361* (6397), 52−57.
(15) Natraj, A.; Ji, W.; Xin, J.; Castano, I.; Burke, D. W.; Evans, A. M.; Strauss, M. J.; Ateia, M.; Hamachi, L. S.; Gianneschi, N. C.; ALOthman, Z. A.; Sun, J.; Yusuf, K.; Dichtel, W. R. Single-Crystalline Imine-Linked Two-Dimensional Covalent Organic Frameworks Separate Benzene and Cyclohexane Efficiently. *J. Am. Chem. Soc.* **2022**, *144*, 19813.
(16) Kang, C.; Yang, K.; Zhang, Z.; Usadi, A. K.; Calabro, D. C.; Baugh, L. S.; Wang, Y.; Jiang, J.; Zou, X.; Huang, Z.; Zhao, D. Growing Single Crystals of Two-Dimensional Covalent Organic Frameworks Enabled by Intermediate Tracing Study. *Nat. Commun.* **2022**, *13* (1), 1370.
(17) Qian, C.; Wu, H.; Teo, W. L.; Liao, Y.; Zhao, Y. Single-Crystalline Covalent Organic Frameworks. *Trends Chem.* **2023**, *5* (11), 853−867.
(18) Massa, W. *Crystal Structure Determination*; Springer: Berlin, Heidelberg, 2004. DOI: 10.1007/978-3-662-06431-3.
(19) Clegg, W.; Clegg, W. *Crystal Structure Determination*; Oxford University Press, 1998.
(20) Dinnebier, R. E. *Powder Diffraction: Theory and Practice*; The Royal Society of Chemistry, 2008. DOI: 10.1039/9781847558237.
(21) Pawley, G. S. Unit-Cell Refinement from Powder Diffraction Scans. *J. Appl. Crystallogr.* **1981**, *14* (6), 357−361.
(22) Fourquet, J. L.; Duroy, H.; Le Bail, A. Ab-Initio Structure Determination of LiSbWO6 by X-Ray Powder Diffraction. *Mater. Res. Bull.* **1988**, *23*, 447.
(23) Rietveld, H. M. A Profile Refinement Method for Nuclear and Magnetic Structures. *J. Appl. Crystallogr.* **1969**, *2* (2), 65−71.
(24) Dinnebier, R. E. Preface: Modern Rietveld Analysis. *Z. Für Krist.* **2011**, *226* (12), V−V.
(25) McCusker, L. B.; Von Dreele, R. B.; Cox, D. E.; Louër, D.; Scardi, P. Rietveld Refinement Guidelines. *J. Appl. Crystallogr.* **1999**, *32* (1), 36−50.
(26) Lukose, B.; Kuc, A.; Heine, T. The Structure of Layered Covalent-Organic Frameworks. *Chem. - Eur. J.* **2011**, *17* (8), 2388−2392.
(27) Haase, F.; Gottschling, K.; Stegbauer, L.; Germann, L. S.; Gutzler, R.; Duppel, V.; Vyas, V. S.; Kern, K.; Dinnebier, R. E.; Lotsch, B. V. Tuning the Stacking Behaviour of a 2D Covalent Organic Framework through Non-Covalent Interactions. *Mater. Chem. Front.* **2017**, *1* (7), 1354−1361.
(28) Zhang, Y.; Položij, M.; Heine, T. Statistical Representation of Stacking Disorder in Layered Covalent Organic Frameworks. *Chem. Mater.* **2022**, *34* (5), 2376−2381.
(29) Wang, Z.; Zhang, Y.; Wang, T.; Lin, E.; Wang, T.; Chen, Y.; Cheng, P.; Zhang, Z. Modulating the Interlayer Stacking of Covalent Organic Frameworks for Efficient Acetylene Separation. *Small* **2023**, *19* (32), 2303684.
(30) Emmerling, S. T.; Schuldt, R.; Bette, S.; Yao, L.; Dinnebier, R. E.; Kästner, J.; Lotsch, B. V. Interlayer Interactions as Design Tool for Large-Pore COFs. *J. Am. Chem. Soc.* **2021**, *143* (38), 15711−15722.
(31) Kuc, A.; Springer, M. A.; Batra, K.; Juarez-Mosqueda, R.; Wöll, C.; Heine, T. Proximity Effect in Crystalline Framework Materials: Stacking-Induced Functionality in MOFs and COFs. *Adv. Funct. Mater.* **2020**, *30* (41), 1908004.
(32) Yang, S.; Li, X.; Qin, Y.; Cheng, Y.; Fan, W.; Lang, X.; Zheng, L.; Cao, Q. Modulating the Stacking Model of Covalent Organic Framework Isomers with Different Generation Efficiencies of Reactive Oxygen Species. *ACS Appl. Mater. Interfaces* **2021**, *13* (25), 29471−29481.
(33) Keller, N.; Calik, M.; Sharapa, D.; Soni, H. R.; Zehetmaier, P. M.; Rager, S.; Auras, F.; Jakowetz, A. C.; Görling, A.; Clark, T.; Bein, T. Enforcing Extended Porphyrin J-Aggregate Stacking in Covalent Organic Frameworks. *J. Am. Chem. Soc.* **2018**, *140* (48), 16544−16552.
(34) You, P.-Y.; Mo, K.-M.; Wang, Y.-M.; Gao, Q.; Lin, X.-C.; Lin, J.-T.; Xie, M.; Wei, R.-J.; Ning, G.-H.; Li, D. Reversible Modulation of Interlayer Stacking in 2D Copper-Organic Frameworks for Tailoring Porosity and Photocatalytic Activity. *Nat. Commun.* **2024**, *15* (1), 194.
(35) Rawat, K. S.; Borgmans, S.; Braeckevelt, T.; Stevens, C. V.; Van Der Voort, P.; Van Speybroeck, V. How the Layer Alignment in Two-Dimensional Nanoporous Covalent Organic Frameworks Impacts Its Electronic Properties. *ACS Appl. Nano Mater.* **2022**, *5* (10), 14377−14387.
(36) Chen, X.; Addicoat, M.; Irle, S.; Nagai, A.; Jiang, D. Control of Crystallinity and Porosity of Covalent Organic Frameworks by Managing Interlayer Interactions Based on Self-Complementary π-Electronic Force. *J. Am. Chem. Soc.* **2013**, *135* (2), 546−549.
(37) Grunenberg, L.; Keßler, C.; Teh, T. W.; Schuldt, R.; Heck, F.; Kästner, J.; Groß, J.; Hansen, N.; Lotsch, B. V. Probing Self-Diffusion of Guest Molecules in a Covalent Organic Framework: Simulation and Experiment. *ACS Nano* **2024**, *18* (25), 16091−16100.
(38) Mähringer, A.; Medina, D. D. Taking Stock of Stacking. *Nat. Chem.* **2020**, *12* (11), 985−987.
(39) Grunenberg, L.; Savasci, G.; Terban, M. W.; Duppel, V.; Moudrakovski, I.; Etter, M.; Dinnebier, R. E.; Ochsenfeld, C.; Lotsch, B. V. Amine-Linked Covalent Organic Frameworks as a Platform for Postsynthetic Structure Interconversion and Pore-Wall Modification. *J. Am. Chem. Soc.* **2021**, *143* (9), 3430−3438.
(40) Warren, B. E. X-Ray Diffraction in Random Layer Lattices. *Phys. Rev.* **1941**, *59* (9), 693−698.
(41) Fang, Q.; Zhuang, Z.; Gu, S.; Kaspar, R. B.; Zheng, J.; Wang, J.; Qiu, S.; Yan, Y. Designed Synthesis of Large-Pore Crystalline Polyimide Covalent Organic Frameworks. *Nat. Commun.* **2014**, *5* (1), 4503.
(42) Zhu, D.; Zhang, J.-J.; Wu, X.; Yan, Q.; Liu, F.; Zhu, Y.; Gao, X.; Rahman, M. M.; Yakobson, B. I.; Ajayan, P. M.; Verduzco, R. Understanding Fragility and Engineering Activation Stability in Two-

Dimensional Covalent Organic Frameworks. *Chem. Sci.* **2022**, *13* (33), 9655−9667.
(43) Evans, A. M.; Ryder, M. R.; Ji, W.; Strauss, M. J.; Corcos, A. R.; Vitaku, E.; Flanders, N. C.; Bisbey, R. P.; Dichtel, W. R. Trends in the Thermal Stability of Two-Dimensional Covalent Organic Frameworks. *Faraday Discuss.* **2021**, *225* (0), 226−240.
(44) Evans, A. M.; Ryder, M. R.; Flanders, N. C.; Vitaku, E.; Chen, L. X.; Dichtel, W. R. Buckling of Two-Dimensional Covalent Organic Frameworks under Thermal Stress. *Ind. Eng. Chem. Res.* **2019**, *58* (23), 9883−9887.
(45) Evans, A. M.; Strauss, M. J.; Corcos, A. R.; Hirani, Z.; Ji, W.; Hamachi, L. S.; Aguilar-Enriquez, X.; Chavez, A. D.; Smith, B. J.; Dichtel, W. R. Two-Dimensional Polymers and Polymerizations. *Chem. Rev.* **2022**, *122* (1), 442−564.
(46) Emmerling, S. T.; Germann, L. S.; Julien, P. A.; Moudrakovski, I.; Etter, M.; Friščić, T.; Dinnebier, R. E.; Lotsch, B. V. *In Situ* Monitoring of Mechanochemical Covalent Organic Framework Formation Reveals Templating Effect of Liquid Additive. *Chem.* **2021**, *7* (6), 1639−1652.
(47) Stähler, C.; Grunenberg, L.; Terban, M. W.; Browne, W. R.; Doellerer, D.; Kathan, M.; Etter, M.; Lotsch, B. V.; Feringa, B. L.; Krause, S. Light-Driven Molecular Motors Embedded in Covalent Organic Frameworks. *Chem. Sci.* **2022**, *13* (28), 8253−8264.
(48) Coelho, A. A. TOPAS and TOPAS-Academic: An Optimization Program Integrating Computer Algebra and Crystallographic Objects Written in C++. *J. Appl. Crystallogr.* **2018**, *51*, 210.
(49) Dinnebier, R. E.; Leineweber, A.; Evans, J. S. O. *Rietveld Refinement: Practical Powder Diffraction Pattern Analysis Using TOPAS*; De Gruyter, 2018. DOI: 10.1515/9783110461381
(50) Cheary, R. W.; Coelho, A. Fundamental Parameters Approach to X-Ray Line-Profile Fitting. *J. Appl. Crystallogr.* **1992**, *25*, 109.
(51) Cheary, R. W.; Coelho, A. A.; Cline, J. P. Fundamental Parameters Line Profile Fitting in Laboratory Diffractometers. *J. Res. Natl. Inst. Stand. Technol.* **2004**, *109*, 1.
(52) Bette, S.; Takayama, T.; Duppel, V.; Poulain, A.; Takagi, H.; Dinnebier, R. E. Crystal Structure and Stacking Faults in the Layered Honeycomb, Delafossite-Type Materials $Ag_3LiIr_2O_6$ and $Ag_3LiRu_2O_6$. *Dalton Trans.* **2019**, *48*, 9250.
(53) Bette, S.; Hinrichsen, B.; Pfister, D.; Dinnebier, R. E. A Routine for the Determination of the Microstructure of Stacking-Faulted Nickel Cobalt Aluminium Hydroxide Precursors for Lithium Nickel Cobalt Aluminium Oxide Battery Materials. *J. Appl. Crystallogr.* **2020**, *53*, 76.

https://doi.org/10.1021/jacsau.4c00979
JACS Au 2025, 5, 388−398